Dispersive Terahertz Gain of a Nonclassical Oscillator: Bloch Oscillation in Semiconductor Superlattices

N. Sekine* and K. Hirakawa†

Institute of Industrial Science, University of Tokyo, 4-6-1 Komaba, Meguro-ku, Tokyo 153-8505, Japan

(Received 11 August 2004; published 11 February 2005)

We have directly determined the spectral shape of the complex conductivities of Bloch oscillating electrons by using the time-domain terahertz (THz) electro-optic sampling technique, and presented experimental evidence for a dispersive Bloch gain in superlattices. This unique dispersive gain without population inversion arises from a nonclassical nature of Bloch oscillations; that is, the phase of the Bloch oscillation is shifted by $\pi/2$ from that of the semiclassical charged harmonic oscillation when driven by the same ac field. By increasing the bias electric field, the gain bandwidth reached ~3 THz in our particular sample.

DOI: 10.1103/PhysRevLett.94.057408 PACS numbers: 78.47.+p, 73.21.Cd, 73.50.Mx, 73.63.Hs

Semiconductor superlattices (SLs) [1], in which two semiconducting materials with different electron affinities are periodically layered by using ultrafine epitaxy technologies, provide an ideal laboratory to study electron transport in solids under high electric fields [2–17]. In SLs, since the energy-momentum (E-k) dispersion for electrons is folded at $k =$ integer multiples of π/d (d, the period of superlattice), a new Brillouin zone which is much narrower than that of the host crystals is formed. Consequently, when dc electric fields are applied to SLs, electrons are easily accelerated to the edge of the reduced Brillouin zone and experience Bragg reflection periodically. As a result, electrons oscillate both in the momentum and the real space, as first predicted by Bloch [18] and Zener [19]. Recent ultrafast laser spectroscopy experiments [13–17] have unambiguously demonstrated that electrons do perform a few cycle Bloch oscillations in SLs, but, at the same time, that the oscillations decay within a few picoseconds. From semiclassical electromagnetism, it is well known that it is not possible to extract a net power from damped charged harmonic oscillators. Because of this automatic thinking, it has often been thought that generation/amplification of terahertz (THz) electromagnetic waves by Bloch oscillators will never be possible.

In contrast to this common anticipation, we would like to show that Bloch oscillators have an essentially different nature from that of semiclassical charged harmonic oscillators and that it is indeed possible to extract a net gain from Bloch oscillations in SLs. By free-space THz electro-optic (EO) sampling method [20,21], we have directly determined the spectral shape of the complex conductivities of Bloch oscillating electrons and confirmed that the real part of the dynamical conductivity goes negative below the Bloch frequency.

In general, damped oscillation of polarization is often described by a charged semiclassical harmonic oscillator, as schematically illustrated in Fig. 1(a). The equation of motion for such a system is expressed as

$$\frac{d^2x(t)}{dt^2} + \Omega^2 x(t) + \frac{1}{\tau}\frac{dx(t)}{dt} = \frac{ef(t)}{m}, \tag{1}$$

where $x(t)$ is the coordinate of the oscillating charge, Ω the eigenfrequency of the charged oscillator, τ the relaxation time, m the mass of the oscillating charge, $f(t)$ the external electric field, and e the elementary charge. It is well known that, if the oscillator is driven by an ac field at a frequency ω, the real part of the complex conductivity, $\mathrm{Re}[\sigma(\omega)]$, has a Lorentzian line shape and the imaginary part of the conductivity, $\mathrm{Im}[\sigma(\omega)]$, is dispersive, as schematically

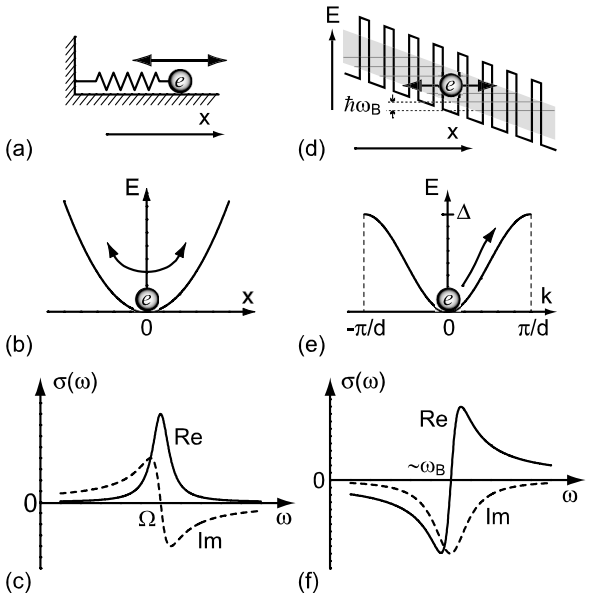

FIG. 1. Comparison between a semiclassical charged harmonic oscillator (HO) and a Bloch oscillator (BO). (a) shows a physical model of a charged HO and (b) is its potential diagram. The complex conductivity spectrum of the charged HO is schematically illustrated in (c). (d), (e), (f) depict an energy band diagram of a biased superlattice, the E-k dispersion curve, and the complex conductivity spectrum of the BO, respectively.

shown in Fig. 1(c). Therefore, the semiclassical charged harmonic oscillator has a maximum loss at its eigenfrequency and no gain can be extracted.

When an appropriate dc electric field F is applied to a SL, electrons are accelerated in the ground miniband, as illustrated in Figs. 1(d) and 1(e). If we approximate the E-k dispersion of the ground miniband by a cosine function [see Fig. 1(e)], electrons in a SL are accelerated as $\hbar\dot{k}(t) = eF$ on a dispersion curve given by $E(k(t)) = \Delta(1 - \cos dk(t))/2$ [$\hbar k(t)$, the crystal momentum of a Bloch oscillating electron and Δ, the miniband width]. Furthermore, the nonequilibrium electron distribution function $g(k, t)$ satisfies the following Boltzmann equation:

$$\frac{\partial g(k,t)}{\partial t} + \frac{eF}{\hbar}\frac{\partial g(k,t)}{\partial k} = \text{scattering term}. \quad (2)$$

If we approximate the scattering term by using an energy- and a momentum-relaxation time, τ_e and τ_m, respectively, and solve Eq. (2) by using the balanced equation method, the following specific equation for the drift velocity of the electron system can be derived [22],

$$\frac{d^2V(t)}{dt^2} + \left(\omega_B^2 + \frac{1}{\tau_e\tau_m}\right)V(t) + \left(\frac{1}{\tau_e} + \frac{1}{\tau_m}\right)\frac{dV(t)}{dt} = \frac{\mu F}{\tau_e\tau_m}, \quad (3)$$

where $V(t)$ is the electron velocity averaged by the distribution function $g(k, t)$, ω_B the Bloch frequency ($= edF/\hbar$), and μ the low-field mobility along the SL axis. When Eq. (3) is compared with Eq. (1), it is noticed that they have almost an identical form. However, there is a crucial difference; that is, Eq. (3) is a differential equation with respect to $V(t)$, whereas Eq. (1) is one with respect to $x(t)$. This means that, when an electric field is applied, electrons both in semiclassical charged harmonic oscillator and in SLs oscillate but with a $\pi/2$-phase difference. This is the essential point of the nonclassical nature of Bloch oscillators. Consequently, the real and the imaginary part of the complex conductivities for semiclassical harmonic oscillators are swapped with each other in SLs. This fact leads to a very important implication that $\mathrm{Re}[\sigma(\omega)]$ of Bloch oscillating electrons becomes dispersive, while $\mathrm{Im}[\sigma(\omega)]$ has a Lorentzian shape, as schematically illustrated in Fig. 1(f). If this is the case, $\mathrm{Re}[\sigma(\omega)]$ of Bloch oscillating electrons becomes negative below $\sim\omega_B$ and Bloch oscillators do have a THz gain.

Very recently, Shimada *et al.* [23] and Savvidis *et al.* [24] have presented strong experimental supports for such a Bloch gain. However, both works did not definitively show negative $\mathrm{Re}[\sigma(\omega)]$. In this work, we have determined the spectral shapes of complex high-frequency conductivities of Bloch oscillating electrons by using time-resolved THz-EO sampling technique and presented strong evidence that Bloch oscillating electrons have a dispersive gain for electromagnetic waves in the THz range.

The samples used in this work were prepared by growing 500 nm thick undoped $GaAs/Al_{0.3}Ga_{0.7}As$ superlattice layers on n^+-GaAs substrates by molecular beam epitaxy. We have studied four different SL structures and obtained basically the same results. Therefore, in this Letter, we will show the results on a SL with 6.5 nm thick GaAs wells and 2.5 nm thick $Al_{0.3}Ga_{0.7}As$ barriers. The ground miniband of this sample was 30 meV wide and was separated from the first excited miniband by a 100 meV wide minigap. The top and the bottom contacts were formed by depositing a semitransparent NiCr Schottky film and AuGeNi/Au layers, respectively. By using these two electrodes, a static bias electric field F was applied to the undoped SL region. When a femtosecond laser pulse excites the sample, electron-hole pairs are optically injected into the miniband. Because of an applied electric field, the carriers start drifting and a THz electromagnetic wave that is proportional to the carrier acceleration is emitted into free space. Since the miniband width for heavy holes is much narrower than that for electrons, heavy holes are almost localized. Furthermore, absorption due to light holes is $1/3$ of that due to heavy holes. Consequently, the motion of electrons dominates the emitted THz signal.

The THz radiation was detected by using THz-EO sampling technique [20,21]. This technique was chosen since the spectral response of electro-optic crystals (EOXs) can be accurately predicted and, if properly designed, THz waveforms can be recorded with small spectral distortion. In our experiment, a 100 μm thick ZnTe crystal was used as the EOX, which has a rather flat response up to 4 THz. In the EOX, a birefringence proportional to the amplitude of an electric field (Pockels effect) is induced by an incident THz radiation. The waveform of the THz electric field was obtained in the time domain by the balanced detection of the probe lights polarized along the two principal axes of the EOX. The pump and the probe pulses were delivered from a mode-locked Ti:sapphire laser (pulse width $\sim$100 fs). The loosely focused pump beam was incident on the SL surface and its power was set to be $\sim$4 mW to minimize the field screening effect by the photoexcited carriers. The pump photon energy was adjusted to be 1.605 eV, which is close to the bottom of the ground miniband [17]. The detection bandwidth of our experimental setup was $\sim$4 THz, which was limited both by the characteristics of our 100 μm thick ZnTe EOX and by the energy uncertainty of the femtosecond pump laser pulses. The sample was cooled at $T = 10$ K.

Figure 2 shows the waveforms of the THz electric field, E_{THz}, emitted from the SL sample measured at various F, ranging from 1 to 39 kV/cm. As seen in the figure, E_{THz} is initially positive and, then, becomes negative. For $9\ \mathrm{kV/cm} < F < 29\ \mathrm{kV/cm}$, clear oscillations appear in the trailing part and their period becomes shorter with increasing F. Since we create electrons close to the bottom of the ground miniband, the photoexcited electrons are first accelerated by the electric field and, subsequently, decelerated when they go beyond the inflection point of the E-k dispersion. They continue this acceleration/deceleration cycle due to periodic Bragg reflection until the coherence

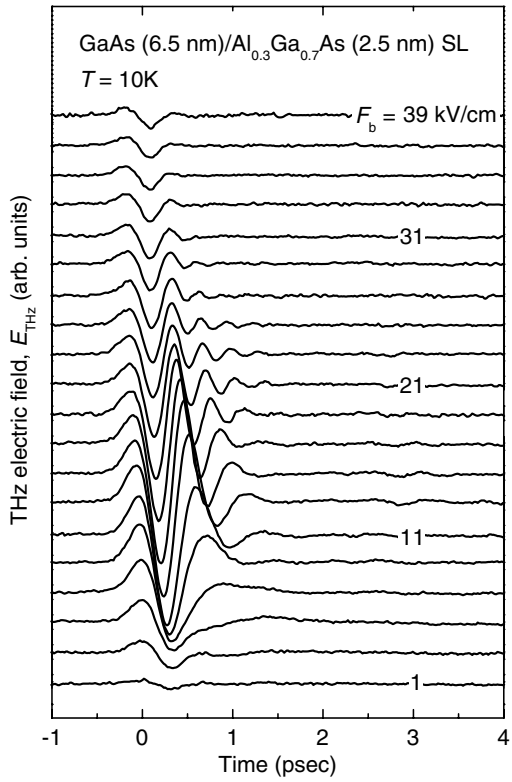

FIG. 2. The waveforms of the THz radiation emitted from the SL sample recorded for various bias electric fields, F (1–39 kV/cm; 2 kV/cm step). The traces are shifted for clarity. For very low electric fields (<3 kV/cm), we had to apply large positive voltages to the surface Schottky junction (for example, $+0.9V$ for $F \sim 1$ kV/cm) and a significant forward bias current (of the order of a few mA) started flowing through the sample. Therefore, we could not obtain reliable THz signals for $F <$ 3 kV/cm due to nonuniformity in the bias electric fields across the sample.

of the oscillation is lost. Such an anticipated behavior is well reproduced in the E_{THz} traces. Furthermore, the oscillation period is roughly consistent with the expected Bloch frequency. A more detailed discussion on the oscillation frequency will be made later. For $F > 25$ kV/cm, the oscillatory behavior gradually vanishes because the oscillation frequency exceeds the bandwidth of our measurement setup.

At this stage, we would like to recall the fact that the time-domain THz emission experiments inherently measure the step response of the electron system to the applied electric field, as described in more detail in Ref. [23]. By noting this important implication, we formulate the THz emission process as follows: the creation of step-function-like carrier density by femtosecond laser pulses in the actual process is replaced with the application of a step-function-like electric field in the thought experiment as

$$F(t) = F\theta(t), \qquad \tilde{F}(s) = F/s, \tag{4}$$

where the variables with ˜ denote their Laplace transformation. The transient current by the photoexcited electrons in the miniband is given by

$$\tilde{J}(s) = \tilde{\sigma}(s)\tilde{F}(s), \tag{5}$$

then the emitted THz electric field E_{THz} can be obtained as

$$E_{\mathrm{THz}}(t) \propto \frac{\partial J(t)}{\partial t} = \frac{1}{2\pi i}\int_{c-i\infty}^{c+i\infty} s e^{ts}\tilde{\sigma}(s)\frac{F}{s}ds = \sigma(t)F, \tag{6}$$

where $\sigma(t)$ is the electron conductivity in the time domain. The important message of Eq. (6) is that the real and the imaginary part of the Fourier spectra of $E_{\mathrm{THz}}(t)/F$ (i. e., $\mathrm{Re}[E_{\mathrm{THz}}(\omega)/F]$ and $\mathrm{Im}[E_{\mathrm{THz}}(\omega)/F]$) are proportional to $\mathrm{Re}[\sigma(\omega)]$ and $\mathrm{Im}[\sigma(\omega)]$, respectively.

Figs. 3(a) and 3(b) show $\mathrm{Re}[E_{\mathrm{THz}}(\omega)/F]$ and $\mathrm{Im}[E_{\mathrm{THz}}(\omega)/F]$ obtained from the experimental data shown in Fig. 2, respectively. In the Fourier transformation process, the position of $t = 0$ is very crucial. We have

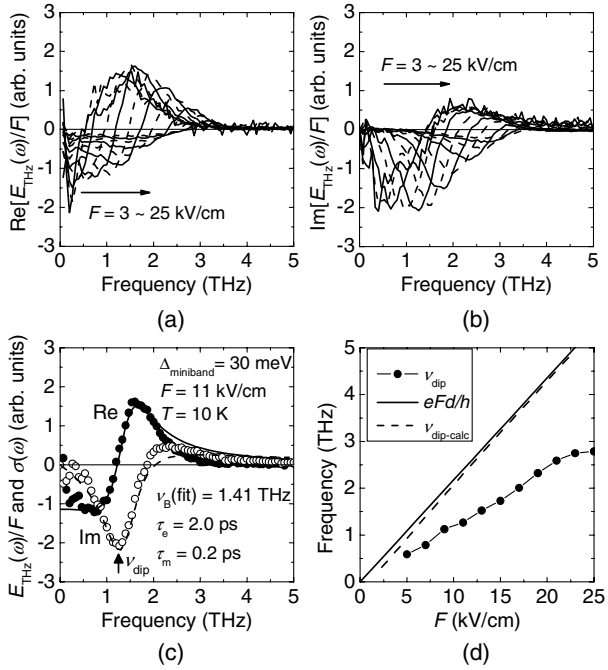

FIG. 3. The real and the imaginary parts of the Fourier spectra of the emitted THz waveforms normalized by F ($= E_{\mathrm{THz}}(\omega)/F$) are shown for various F (3–25 kV/cm, 2 kV/cm step) in (a) and (b), respectively. Since the critical field for the onset of negative differential conductivity F_c of this sample is $\sim$1.2 kV/cm, the minimum electric field plotted in (a) and (b) already exceeds F_c. In (c), a typical $E_{\mathrm{THz}}(\omega)/F$ is picked up ($F = 11$ kV/cm; full and open circles) and compared with the conductivity spectrum calculated by using a theory developed by Ktitorov *et al.* (solid and dashed lines) (Ref. [3]). The parameters used in the calculation are listed in the lower right of the figure. (d) compares the dip frequency (ν_{dip}, dots) with the Bloch frequency ($\equiv edF/h$, line). Since edF/h was determined by dividing the applied voltage by the number of period of the SL (55 for the present sample), it is free from the error in the layer thickness of the sample. The dip frequency, $\nu_{\mathrm{dip\text{-}calc}}$, calculated by taking account of the effect of scattering (Ref. [3]) is also plotted by a dashed line.

determined $t = 0$ by finding the position where artificial phase jumps in the Fourier spectra do not appear. By doing so, $t = 0$ could be determined within a phase error of $\pm\pi/9$. As expected from the previous discussion, $\mathrm{Re}[E_{\mathrm{THz}}(\omega)/F]$ indeed has a dispersive curve and shows a negative value up to $\sim$3 THz. This is clear experimental evidence for the dispersive Bloch gain in SLs. At the crossover frequency where the $\mathrm{Re}[E_{\mathrm{THz}}(\omega)/F]$ trace changes its polarity from negative to positive, $\mathrm{Im}[E_{\mathrm{THz}}(\omega)/F]$ shows a clear dip (we will call this frequency ν_{dip}). It is noticed that the spectral shape of $\mathrm{Im}[E_{\mathrm{THz}}(\omega)/F]$ is not a simple Lorentzian. This is because Eq. (3) was derived by assuming a constant bias electric field for simplicity. If we take into account an effect of a small ac drive field within a linear response regime, the spectral shapes of $\sigma(\omega)$ are slightly affected. In Fig. 3(c), a typical example of the measured complex conductivity spectrum is picked up ($F = 11$ kV/cm) and compared with a theory that takes into account a small ac drive field [3]. The parameters used in the calculation were chosen to obtain a best fit to the experimental data. It should be noted that the measured $\sigma(\omega)$ spectrum is in excellent agreement with theory.

In Fig. 3(d), ν_{dip} of $\mathrm{Im}[E_{\mathrm{THz}}(\omega)/F]$ and the expected Bloch frequency, ν_B ($\equiv edF/h$), are plotted as a function of F. As seen in the figure, ν_{dip} is significantly ($\sim$40%) smaller than ν_B. We believe this discrepancy originates from at least two factors; one comes from the fact that ν_{dip} deviates from ν_B due to a rather short τ_m in actual SLs [22,25]. This effect was estimated by calculating the conductivity spectra for various F, as done in Fig. 3(c). The calculated dip frequency, $\nu_{\mathrm{dip\text{-}calc}}$, was plotted by a dashed line in Fig. 3(d). Although scattering indeed suppresses the dip frequency below ν_B, its effect is less than 10% (typically, only a few %). The other factor is the excitonic effect [26]. Since both electrons and holes are excited in our experiment, the excitonic effect cannot be neglected and leads to a reduction in the energy separation between the Wannier-Stark levels by a few meV [26]. As a result, ν_{dip} becomes smaller than ν_B.

In summary, we have directly determined the spectral shape of the complex conductivities of Bloch oscillating electrons by using the time-domain THz-EO sampling technique, and presented experimental evidence for a dispersive Bloch gain in SLs. This unique dispersive gain without population inversion arises from a nonclassical nature of Bloch oscillations; that is, the phase of the Bloch oscillation is shifted by $\pi/2$ from that of the semiclassical charged harmonic oscillation when driven by the same ac field. By increasing the bias electric field, the gain bandwidth reached $\sim$3 THz in our particular sample. This result strongly encourages an idea of Bloch oscillators/amplifiers, which are frequency tunable from a few hundred GHz to a few THz and cover a low-THz frequency range that is not easily accessible by quantum cascade lasers [27–29].

We thank K. A. Chao, M. Odnoblyudov, Z. S. Ma, and K. Jin for very fruitful discussions, and L. Esaki, H. Sakaki, Y. Arakawa, and S. Komiyama for encouragement. This work was supported by the Grant-in-Aid from Japan Society for the Promotion of Science (No. 15206037 and No. 16760272), SORST of the Japan Science and Technology Corporation, the Grant-in-Aid for COE research (No. 12CE2004), and the IT program from MEXT.

*Electronic address: nsekine@iis.u-tokyo.ac.jp
†Electronic address: hirakawa@iis.u-tokyo.ac.jp

[1] L. Esaki and R. Tsu, IBM J. Res. Dev. **14**, 61 (1970).
[2] R. F. Kazarinov and R. A. Suris, Sov. Phys. Semicond. **5**, 174 (1971).
[3] S. A. Ktitorov, G. S. Simin, and V. Ya Sindalovskii, Sov. Phys. Solid State **13**, 1872 (1972).
[4] A. A. Ignatov, K. F. Renk, and E. P. Dodin, Phys. Rev. Lett. **70**, 1996 (1993).
[5] E. E. Mendez, F. Agullo-Rueda, and J. M. Hong, Phys. Rev. Lett. **60**, 2426 (1988).
[6] P. Voisin *et al.*, Phys. Rev. Lett. **61**, 1639 (1988).
[7] S. J. Allen *et al.*, Semicond. Sci. Technol. **7**, B1 (1992).
[8] M. Helm, Semicond. Sci. Technol. **10**, 557 (1995).
[9] K. Unterrainer *et al.*, Phys. Rev. Lett. **76**, 2973 (1996).
[10] E. Schomburg *et al.*, Phys. Rev. B **58**, 4035 (1998).
[11] G. Bastard and R. Ferreira, C. R. Acad. Sci., Ser. II: Mec., Phys., Chim., Sci. Terre Univers. **312**, 971 (1991).
[12] H. Kroemer, cond-mat/0007428.
[13] J. Feldmann *et al.*, Phys. Rev. B **46**, 7252 (1992).
[14] C. Waschke *et al.*, Phys. Rev. Lett. **70**, 3319 (1993).
[15] T. Dekorsy *et al.*, Phys. Rev. B **50**, 8106 (1994).
[16] F. Löser *et al.*, Phys. Rev. B **61**, 13373 (2000).
[17] Y. Shimada, K. Hirakawa, and S.-W. Lee, Appl. Phys. Lett. **81**, 1642 (2002).
[18] F. Bloch, Z. Phys. **52**, 555 (1928).
[19] C. Zener, Proc. R. Soc. London A **145**, 523 (1934).
[20] Q. Wu and X.-C. Zhang, Appl. Phys. Lett. **71**, 1285 (1997).
[21] A. Leitenstorfer *et al.*, Appl. Phys. Lett. **74**, 1516 (1999).
[22] A. A. Ignatov, E. P. Dodin, and V. I. Shashkin, Mod. Phys. Lett. B **5**, 1087 (1991).
[23] Y. Shimada, K. Hirakawa, M. Odnoblioudov, and K. A. Chao, Phys. Rev. Lett. **90**, 046806 (2003).
[24] P. G. Savvidis *et al.*, Phys. Rev. Lett. **92**, 196802 (2004).
[25] N. Sekine, Y. Shimada, K. Hirakawa, Appl. Phys. Lett. **83**, 4794 (2003).
[26] M. M. Dignam and J. E. Sipe, Phys. Rev. Lett. **64**, 1797 (1991).
[27] J. Faist *et al.*, Science **264**, 553 (1994).
[28] R. Kohler *et al.*, Nature (London) **417**, 156 (2002).
[29] S. Kumar *et al.*, Appl. Phys. Lett. **84**, 2494 (2004).